Finite-Element Model for Wood-Based Floors with Lateral Reinforcements

Lei Jiang[1]; Lin Hu[2]; and Ying-Hei Chui[3]

Abstract: Lateral reinforcements can enhance serviceability of wood-based floor systems. However, because of a lack of proper analysis models, the benefit from installing these components has not been fully recognized in floor design. In this paper, a finite-element model for predicting static and dynamic characteristics of wood-based floor structures with various types of lateral reinforcements is presented. In this model, shell elements were employed to represent floor decking and ceiling, and beam elements were utilized to model joists and structural members in the lateral reinforcements. Special connector elements were developed to model the fasteners connecting various structural components. Other structural features, such as gaps perpendicular to joists in the subfloor, additional objects on floor and flexible supports, were also considered. A computer model incorporating these new features has been developed. For verification and validation purposes, the predicted deflections and natural frequencies for a number of full-size floors were compared with experimental values. Good agreement has been observed. These numerical test results indicated that the present finite-element model is reliable and unique, particularly in modeling floors with lateral reinforcements.

DOI: 10.1061/(ASCE)0733-9445(2004)130:7(1097)

CE Database subject headings: Finite element method; Wood floors; Structural reinforcement; Fasteners; Connections; Joints; Connections, semi-rigid.

Introduction

A wood-based floor system normally consists of wood joists and a wood subfloor as essential structural components. Various types of topping and ceiling may also be used to improve its acoustic and fire performance. Fig. 1 illustrates a typical wood-based floor system. This system may be further reinforced in the across-joist direction using various lateral components, such as blocking, strong back, cross bridging, bracing, and strapping, as shown in Figs. 2(a–e). These lateral reinforcements are usually attached to joists using mechanical fasteners.

Effective serviceability design of wood-based floors depends on the availability of proper serviceability criteria, reliable calculation procedures, and accurate design specifications for the various floor components. Comprehensive mathematical models, which are capable of predicting static deflections and natural frequencies of wood-based floor structures, are required not only as a design tool, but also for benchmarking any simplified design equations used routinely by design engineers. Furthermore, these models are powerful tools for the development of innovative floor components and systems. However, due to the complexity of wood-based floor systems, engineers and researchers are faced with many challenges when developing reliable comprehensive mathematical models to analyze such systems. Difficulties involved in accurate modeling of the wood-based floor systems arise from various complexities in such structures, including:

1. Significant transverse shear deformations in joists due to the low ratio of shear-to-bending stiffness;
2. Gaps in subfloor, over which discontinuities exist in displacement and its spatial derivatives;
3. Composite anisotropic material properties of wood subfloor and ceiling panels;
4. Semi-rigid connections between subfloor and joists;
5. Additional objects on floor surface such as partition walls, furniture, and human bodies;
6. Various forms of lateral reinforcements, which are semi-rigidly fastened to the joists; and
7. Semi-rigid joist end support conditions arising from the use of floor beams and lintels.

Many efforts have been made to develop reliable mathematical models for analyzing wood-based floors. One of the first attempts was by Thompson and his co-workers who proposed a multilayered beam finite element model for static analysis of wood floor (Thompson et al. 1975). In their method, a floor was divided into a collection of crossing T-beams. Each beam was composed of a single joist and the associated subfloor. These crossing beams were then analyzed individually using beam element discretization in the axial direction. Load–slip moduli of the connections between joist and subfloor and between layers in the subfloor were introduced into the model through a smeared stiffness concept to account for the effect of shear deformations in these connections. To establish the kinematic relations at the connecting interface, the rotations associated with vertical bending were assumed to be identical in joist and subfloor. The gaps in subfloor were modeled by two methods. The first method was for open

[1]Senior Research Engineer, Martec Limited, 400-1888 Brunswick St., Halifax NS, Canada B3J 2J8 (corresponding author). E-mail: ljiang@martec.com

[2]Research Scientist, Forintek Canada Corp., 319 rue Franquet, Saint-Foy PQ, Canada G1P 4R4.

[3]Professor, Faculty of Forestry and Environment Management, Univ. of New Brunswick, Fredericton NB, Canada E3B 5A3.

Note. Associate Editor: Marc I. Hoit. Discussion open until December 1, 2004. Separate discussions must be submitted for individual papers. To extend the closing date by one month, a written request must be filed with the ASCE Managing Editor. The manuscript for this paper was submitted for review and possible publication on May 20, 2002; approved on September 10, 2003. This paper is part of the ***Journal of Structural Engineering***, Vol. 130, No. 7, July 1, 2004. ©ASCE, ISSN 0733-9445/2004/7-1097–1107/$18.00.

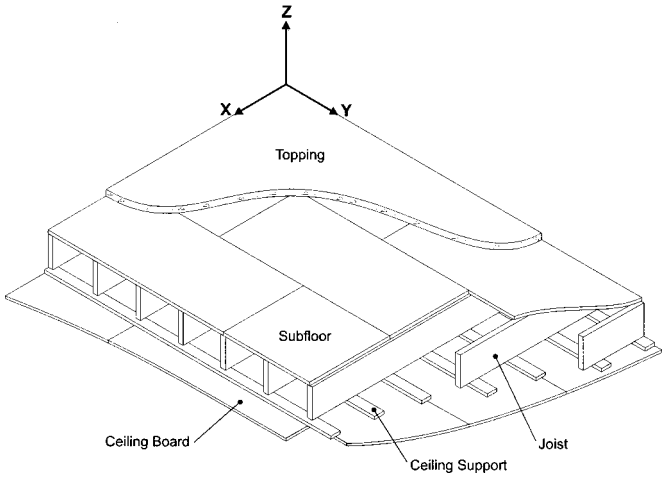

Fig. 1. Typical wood-based floor system

gaps. In this method, two nodes were generated with the same coordinates at both sides of a gap. This approach permitted displacement discontinuities and zero axial forces across gaps and could be viewed as a special element having a zero length. The second method involved use of regular finite elements but with a small length and a low modulus of elasticity. This method was suitable for representing glue-filled or tightly butted gaps. Thompson et al. (1975) compared static deflections predicted by their model with the measured values from limited laboratory testing and good agreement was obtained. The most significant contribution of the work by Thompson et al. was the introduction of the concept of load–slip modulus for accounting for the semirigid attachments between various structural components. However, because lateral deformations of the subfloor and interactions between the adjacent crossing beams were completely ignored in this model, torsion of joist and lateral bending of subfloor could not be taken into account. This simplification leads to overly conservative predictions of deflections. For the same reason, lateral reinforcements cannot be included in that model. Finally, that model was only developed and tested for static analyses, but not for dynamic problems.

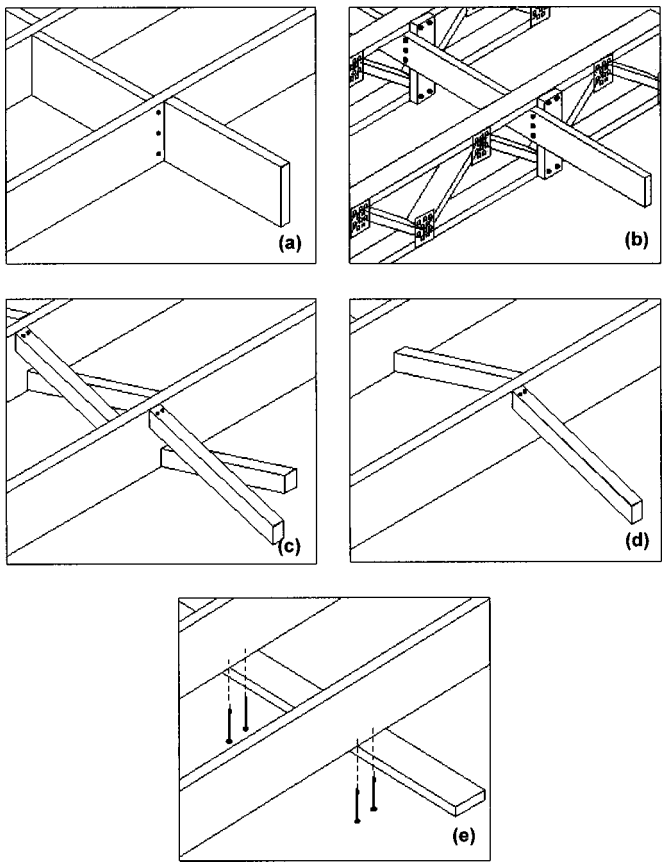

Fig. 2. Typical lateral reinforcements: (a) blocking, (b) strong back, (c) bridging, (d) bracing, and (e) strapping

Foschi (1982) presented a finite strip model for static analysis of wood-based floors. In his model, standard finite-element discretization was utilized in the lateral direction and harmonic functions were employed to describe displacement variations in the axial direction. Slips at the subfloor-to-joists connections were considered using a smeared stiffness approach similar to that of Thompson et al. (1975). Due to the inclusion of lateral deformations, the Foschi floor model could incorporate the effects of torsion of joists and flexible end support conditions without difficulty. However, the transverse shear deformation of the joists was not included. The original Foschi model for static analysis was later extended to predict natural frequencies (Filiatrault et al. 1990) and dynamic responses (Gupta 1985; Foschi and Gupta 1987; Folz and Foschi 1991) of wood floors. Although Foschi's model had been successfully applied to various floor designs, it still suffered from some limitations. The use of harmonic functions for describing displacement variations in the joist direction preassumed continuity in displacements and their spatial derivatives and as a result, did not provide the flexibility for accurate modeling of complicated deformation patterns. For example, gaps in subfloor were considered by simply eliminating the gap width from the integration range in element stiffness computations. However, proper displacement discontinuity across the gaps was still not achieved. For the same reason, accurate representation of lateral reinforcements was also not permissible in this model. Foschi suggested a simplified approach for modeling lateral reinforcements by completely restricting the out-of-plane rotation of the joists. Such an approach only enabled the model to account for the maximum contribution of lateral components, and had the possibility of significantly overestimating their contributions. In addition, the effect of lateral reinforcements on restraining relative vertical displacements of joists was ignored. Hu (1992) has also demonstrated that for floors with joists having low shear rigidity, the use of Foschi's model resulted in higher natural frequencies than the experimental data.

Chui (1987) presented a Rayleigh–Ritz model for frequency and dynamic response analyses of wood-based floors. Semirigid connection between joists and subfloor was considered using the approximate method developed by Smith (1980), but gaps in subfloor were ignored. Hu (1992) presented a modal synthesis method for predicting frequency and dynamic responses of wood-based floors. In addition to the parameters in other models, shear deformation and rotatory inertia of joists were included in her analysis. Hu (1992) reported that the model provided better predictions of natural frequencies of wood floors with joists having low ratio of shear-to-bending stiffness than Foschi's and Chui's models. Unfortunately, none of these models are able to consider properly the influence of lateral reinforcements.

Berkoh (1997) proposed an improved modal synthesis method, which includes a more complete set of deformation modes, gaps perpendicular to joists in subfloor, flexible joist supports, and lateral reinforcements. In his model, continuous lateral reinforce-

ments, such as strong back and strapping, were considered as bending substructures of the subfloor. However, the stiffness of the lateral reinforcements was not clearly defined. This ambiguity made data preparation very difficult in practical engineering computations. Berkoh reported that compared with Hu's model, his model predicted more accurate natural frequencies for the higher vibration modes.

Parallel to the development of numerical models, Onysko (1981) developed a semianalytical model based on the approach of Vermeyden (1968) to predict the static deflections of wood-based floors under a concentrated load. This approach assumed that a loaded joist shared an applied concentrated load with the adjacent joists on both sides. The approximate formula proposed by McCutcheon (1977) was adopted to account for the effects of partial composite action between joists and subfloor and the gaps perpendicular to joists in the subfloor. This model included lateral reinforcements. The continuous lateral reinforcements, such as strapping [Fig. 2(e)] and strong back [Fig. 2(b)], were considered as bending elements, and the discrete lateral reinforcements, such as bridging [Fig. 2(c)] and blocking [Fig. 2(a)], as shear elements. The equivalent shear modulus was back calculated from the measured static deflections by solving a set of nonlinear equations. This semianalytical model was formed as a benchmark for the design criterion and procedure for solid lumber joist floors in Part 9 of the National Building Code of Canada [National Research Council (NRC) 1995]. Onysko reported that the concentrated load deflections predicted by the model agreed reasonably well with the measured values from floor testing. However, this model has a number of limitations. For example, strictly this model is only applicable to floors with seven joists with two free edges. The determination of equivalent shear modulus requires complicated experiments and computations, and it is still unclear whether the equivalent shear modulus determined from a particular floor specimen can be generalized to other types of floor systems. In addition, this model is limited to static deflection analysis, not for dynamic analysis.

The above literature review indicates that all the existing analytical and numerical models are working reasonably well on certain floor systems which are consistent with the assumptions used in the development of these models. However, none of them can meet all the challenges listed earlier in this section. The review also revealed that at the present time, there is no reliable and effective model for characterizing the effects of lateral reinforcements. To better understand the mechanism of these structural components, a more appropriate numerical model must be developed. To this end, the finite-element method seems to be a logical option due to its flexibility, generality, and reliability.

Commercially available general-purpose finite-element programs have recently been utilized to analyze wood-based floor systems (Beattie 1998). However, because these commercial finite-element packages provide neither specialized connector elements for representing the fasteners nor customized user interface for wood-based floor structures, model generation could be very time consuming. Furthermore, because each fastener must be modeled using an individual three-dimensional spring element, local mesh density of the finite-element model is dictated by the fastener spacing and as a result, unnecessarily refined meshes are often generated, resulting in excessive computational times.

In this paper, a specially customized finite element procedure is developed to address most of the complexities existing in wood-based floor systems. These include transverse shear deformations, multilayered subfloor and ceiling, gaps perpendicular to joists in subfloor, semirigid fastener connections, rigid and flexible support conditions, and most importantly, various types of lateral reinforcements.

The present development has been based on extension of an existing general-purpose finite element program *VAST* (Martec Limited 2000). This program was first developed in the early 1970s and has been continuously enhanced in the past 3 decades. It has been verified extensively and applied to numerous practical engineering problems. Various shell and beam elements, which are suitable for representing subfloor and joists, already exist in *VAST*. In the present work, special connector elements are developed in *VAST* to model the semirigid connections between the subfloor and joists, and between joists and the lateral components. User friendly special-purpose pre- and postprocessing capabilities have also been developed for wood-based floors.

The organization of the present paper is as follows. The next section is devoted to detailed presentation of finite element formulations for the shell, beam, and connector elements. Numerical verification of the developed finite element analysis capability is then presented, in which predicted static deflections and natural frequencies are compared with the experimental measurements.

Finite Element Formulations and Development of Model

Four-Noded Shell Element with Multilayered Composite Capability

The four-noded quadrilateral shell element utilized in the present wood floor model was developed based on the degenerated three-dimensional isoparametric solid element approach (Aham et al. 1970). One of the most significant advantages of this element formulation is that it includes transverse shear deformations, and as a result, can be applied to both thin and moderately thick shell structures, and especially for shells with a low shear rigidity, such as the wood panels. Making use of the geometric and displacement expressions, the strain–displacement matrix **B** can be derived following the standard procedure for constructing isoparametric finite element. However, a shell element formulated this way exhibits a serious numerical problem, known as shear ''locking.'' A number of methods have been developed to eliminate the locking problem and one of the most successful methods is the technique of mixed interpolation of tensorial strain component developed by Dvorkin and Bathe (1984). In this method, the strain–displacement matrix was first formulated in terms of the covariant strain components in the parametric coordinate system. The covariant transverse shear strain components were then modified through a mixed interpolation. Finally, the modified covariant strain–displacement matrix is transformed back to the desired orthogonal coordinate system, in which the element stresses and strains are formulated.

Once the **B** matrix is available, the element stiffness matrix can be formulated as

$$\mathbf{K} = \int_V \mathbf{B}^T \mathbf{D} \mathbf{B} \, dV \tag{1}$$

where $\mathbf{D}$=elasticity matrix and V=volume of the element. For orthotropic materials, such as the wood panels, the elasticity matrix can be expressed as

$$\mathbf{D}=\begin{bmatrix} \frac{E_X}{1-\nu_{XY}\nu_{YZ}} & \frac{\nu_{XY}E_Y}{1-\nu_{XY}\nu_{YZ}} & 0 & 0 & 0 \\ & \frac{E_Y}{1-\nu_{XY}\nu_{YZ}} & 0 & 0 & 0 \\ & & G_{XY} & 0 & 0 \\ & & & G_{YZ} & 0 \\ \text{Sym.} & & & & G_{ZX} \end{bmatrix} \quad (2)$$

where E_X, E_Y denote the elastic moduli in the principal material directions x and y; ν_{XY}=Poisson's ratio for transverse strain in the y direction when stressed in the x direction; and G_{XY}, G_{YZ}, and G_{ZX}=in-plane and transverse shear moduli, respectively.

For multilayered composite shells with a rigid bond between layers, the elasticity matrix can be expressed as a piecewise constant function of the through-the-thickness coordinate z as

$$\mathbf{D}(z)=\mathbf{D}_i \quad \text{for } z\in[z_{i-1},z_i] \quad (3)$$

where z_{i-1}, z_i denote through-the-thickness coordinates of the lower and upper surfaces of the ith layer. Substituting Eq. (3) into Eq. (1), the stiffness matrix expression for a composite shell element is obtained. In the present implementation, numerical integration is performed in the thickness direction.

Two-Noded Beam Element

The two-noded general beam element utilized in the present finite-element model was developed using cubic shape functions, which satisfy not only displacement compatibility, but also slope continuity across element boundaries. In this element, stiffness matrices corresponding to longitudinal, torsional, and bending deformations are first formulated separately and then superimposed to form the element stiffness matrix. Although this beam element was originally derived using Euler–Bernoulli's beam theory, in which the transverse shear deformation is neglected, its stiffness matrix had been properly modified to take into account the transverse shear effect of beams having relatively deep cross sections and/or low ratios of shear-to-bending rigidity. This modification was based on the so-called shear form factor F, which is the ratio of the total cross sectional area to the effective shear area, such that $F=A/A_S$. The effective shear area A_S is defined in such a way that the transverse shear-induced vertical deflection v_S can be expressed as

$$\frac{dv_S}{dx}=\frac{S}{GA_S} \quad (4)$$

where x=coordinate along the axial direction of the beam; S=transverse shear force; and G=shear modulus (Przemieniecki 1968). For regular cross sections, the shear form factors are either constant or dependent on the cross-sectional dimensions. For instance, for a solid rectangular cross section, $F=6/5$, and for an I section with flanges of uniform thickness (Young and Budynas 2002)

$$F=\left[1+\frac{3(D_2^2-D_1^2)D_1}{2D_2^3}\left(\frac{t_2}{t_1}-1\right)\right]\frac{4D_2^2}{10R^2} \quad (5)$$

where D_1 and D_2 denote distances from the neutral axis to the nearest surface of the flanges and the extreme fiber, respectively; t_1 denotes the thickness of the web; t_2=width of the flange; and R=radius of gyration of the cross section with respect to the neutral axis. If the beam element is defined by cross-sectional properties the transverse shear stiffness, which is the product of the shear modulus and the effective shear area GA_S, must be provided directly.

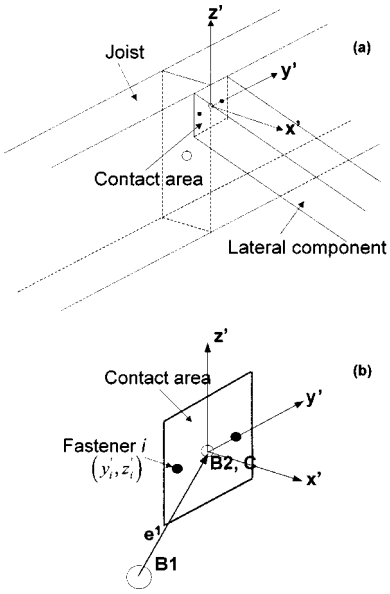

Fig. 3. (a) Typical two-noded interface element for connection between two beams and (b) details of contact area

Two-Noded Connector Element

In order to develop a two-noded connector element suitable for modeling semi-rigid connections between joists and lateral reinforcement members, a beam–beam connection as shown in Fig. 3 was considered. In this figure, a local coordinate system is shown, in which the local x' axis is along the axial direction of the fasteners, whereas the local y' and z' are along the principal axes of the contact area. The origin of the local coordinate system is at the center of the contact area.

Assuming that the local displacement and rotation components at the center of the connecting area are $\{u_1,v_1,w_1,\alpha_1,\beta_1,\gamma_1\}$ and $\{u_2,v_2,w_2,\alpha_2,\beta_2,\gamma_2\}$ for beam nodes $B1$ and $B2$, respectively, the displacements at an arbitrary point (y',z') over this area can be readily expressed as

$$\begin{Bmatrix} u \\ v \\ w \end{Bmatrix}_{C1}=\begin{Bmatrix} u_1 \\ v_1 \\ w_1 \end{Bmatrix}+\begin{bmatrix} 0 & z' & -y' \\ -z' & 0 & 0 \\ y' & 0 & 0 \end{bmatrix}\begin{Bmatrix} \alpha_1 \\ \beta_1 \\ \gamma_1 \end{Bmatrix} \quad (6a)$$

and

$$\begin{Bmatrix} u \\ v \\ w \end{Bmatrix}_{C2}=\begin{Bmatrix} u_2 \\ v_2 \\ w_2 \end{Bmatrix}+\begin{bmatrix} 0 & z' & -y' \\ -z' & 0 & 0 \\ y' & 0 & 0 \end{bmatrix}\begin{Bmatrix} \alpha_2 \\ \beta_2 \\ \gamma_2 \end{Bmatrix} \quad (6b)$$

To derive these relations, the shape of the contact area was assumed to be unchanged during the small elastic deformation. This simplification is consistent with the basic assumptions adopted in the classical beam theory.

Subtracting the displacements on both sides of the connecting surface given in Eqs. (6*a*) and (6*b*), relative displacements experienced by the fasteners in the present connection are readily obtained as

$$\begin{Bmatrix} \Delta u \\ \Delta v \\ \Delta w \end{Bmatrix}_C = \begin{Bmatrix} u_1 - u_2 \\ v_1 - v_2 \\ w_1 - w_2 \end{Bmatrix} + y' \begin{Bmatrix} -\gamma_1 + \gamma_2 \\ 0 \\ \alpha_1 - \alpha_2 \end{Bmatrix} + z' \begin{Bmatrix} \beta_1 - \beta_2 \\ -\alpha_1 + \alpha_2 \\ 0 \end{Bmatrix}$$

$$= \Delta_1 + y' \Delta_2 + z' \Delta_3 \tag{7}$$

where Δ_1, Δ_2, Δ_3 denote vectors of relative displacements and rotations at the center of the connecting area. The total strain energy corresponding to the deformation of the fasteners in the present connection can be expressed in terms of the relative displacements and the connector stiffnesses as

$$U = \frac{1}{2} \int_{A'} [\Delta_1 + y' \Delta_2 + z' \Delta_3]^T \mathbf{k}(y', z') [\Delta_1 + y' \Delta_2 + z' \Delta_3] dA' \tag{8}$$

where A' denotes the area of the connecting surface and

$$\mathbf{k}(y', z') = \begin{bmatrix} k_{x'} & 0 & 0 \\ 0 & k_{y'} & 0 \\ 0 & 0 & k_{z'} \end{bmatrix} \tag{9}$$

contains the connector's axial and slip moduli at an arbitrary point (y', z'). Noting that the relative displacements and rotations Δ_1, Δ_2, Δ_3 are independent of the local coordinates and the local y', z' axes are along the principal directions of the connecting area, the strain energy expression can be simplified as

$$U = \tfrac{1}{2} \Delta_1^T \overline{\mathbf{k}} \Delta_1 + \tfrac{1}{2} \Delta\alpha k_\alpha \Delta\alpha + \tfrac{1}{2} \Delta\beta k_\beta \Delta\beta + \tfrac{1}{2} \Delta\gamma k_\gamma \Delta\gamma \tag{10}$$

where the equivalent translational and rotational stiffness components can be evaluated by summing up the stiffness contributions of each individual fastener in the current connection as

$$\begin{aligned} \overline{\mathbf{k}} &= \sum \mathbf{k}_i \\ k_\alpha &= \sum (y_i'^2 k_{z'i} + z_i'^2 k_{y'i}) \\ k_\beta &= \sum (z_i'^2 k_{x'i}) \\ k_\gamma &= \sum (y_i'^2 k_{x'i}) \end{aligned} \tag{11}$$

and $\mathbf{k}_i$ denotes the 3×3 diagonal stiffness matrix of the ith fastener as given in Eq. (9). In Eq. (10), the strain energy is expressed in terms of the displacements and rotations at the center of the connecting area. However, to derive the stiffness matrix of the two-noded connector element, these displacements and rotations need to be expressed by the displacement and rotation components at the beam nodes, $B1$ and $B2$. For the connection detail shown in Fig. 3(b), if the vector pointing from the beam node $B1$ to the center of the contact area is $\mathbf{e}^1 = [e^1_{x'}, e^1_{y'}, e^1_{z'}]^T$, measured in the local coordinate system, the displacements and rotations can be related as

$$\begin{Bmatrix} u_1 \\ v_1 \\ w_1 \end{Bmatrix} = \begin{Bmatrix} u_{B1} \\ v_{B1} \\ w_{B1} \end{Bmatrix} + \begin{bmatrix} 0 & e^1_{z'} & -e^1_{y'} \\ -e^1_{z'} & 0 & e^1_{x'} \\ e^1_{y'} & -e^1_{x'} & 0 \end{bmatrix} \begin{Bmatrix} \alpha_{B1} \\ \beta_{B1} \\ \gamma_{B1} \end{Bmatrix}$$

$$\begin{Bmatrix} \alpha_1 \\ \beta_1 \\ \gamma_1 \end{Bmatrix} = \begin{Bmatrix} \alpha_{B1} \\ \beta_{B1} \\ \gamma_{B1} \end{Bmatrix} \tag{12}$$

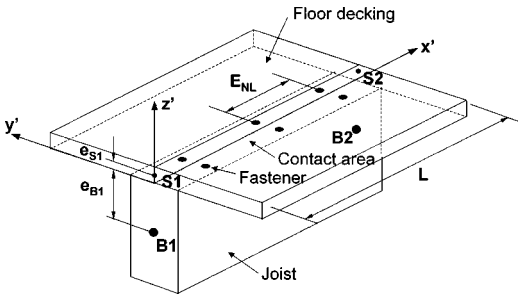

Fig. 4. Four-noded interface element for connection between shell and beam

Similar relations can be established for beam node $B2$. For the special situation shown in Fig. 3(b), beam node $B2$ coincides with the center of the contact area so $\mathbf{e}^2 = \mathbf{0}$. Using Eq. (12), the relative displacements and rotations at the center of the connecting area can be readily written in terms of the displacements and rotations of the beam nodes. In matrix form, we have

$$\begin{Bmatrix} \Delta u \\ \Delta v \\ \Delta w \end{Bmatrix} = \boldsymbol{\Delta}_1 = \mathbf{B} \;\; \mathbf{U} = [\mathbf{I} \;\; \mathbf{E}^1 \;\; -\mathbf{I} \;\; -\mathbf{E}^2]\mathbf{U} \tag{13}$$

for relative displacements where

$$\mathbf{U} = [u_{B1} \; v_{B1} \; w_{B1} \; \alpha_{B1} \; \beta_{B1} \; \gamma_{B1} \; u_{B2} \; v_{B2} \; w_{B2} \; \alpha_{B2} \; \beta_{B2} \; \gamma_{B2}]^T \tag{14}$$

$$\mathbf{E}^i = \begin{bmatrix} 0 & e^i_{z'} & -e^i_{y'} \\ -e^i_{z'} & 0 & e^i_{x'} \\ e^i_{y'} & -e^i_{x'} & 0 \end{bmatrix}, \quad i = 1,2 \tag{15}$$

and $\mathbf{I}$ denotes a 3×3 identity matrix. Similarly, the relative rotations at the center of the connecting area can also be expressed in terms of the displacements and rotations of the beam nodes as

$$\begin{aligned} \Delta\alpha &= \mathbf{H}_1\mathbf{U} = [0 \;\; 0 \;\; 0 \;\; 1 \;\; 0 \;\; 0 \;\; 0 \;\; 0 \;\; 0 \;\; -1 \;\; 0 \;\; 0]\mathbf{U} \\ \Delta\beta &= \mathbf{H}_2\mathbf{U} = [0 \;\; 0 \;\; 0 \;\; 0 \;\; 1 \;\; 0 \;\; 0 \;\; 0 \;\; 0 \;\; 0 \;\; -1 \;\; 0]\mathbf{U} \\ \Delta\gamma &= \mathbf{H}_3\mathbf{U} = [0 \;\; 0 \;\; 0 \;\; 0 \;\; 0 \;\; 1 \;\; 0 \;\; 0 \;\; 0 \;\; 0 \;\; 0 \;\; -1]\mathbf{U} \end{aligned} \tag{16}$$

Substituting Eqs. (13) and (16) into (10), a 12×12 stiffness matrix for the two-noded connector element can be obtained in the local coordinate system as

$$\mathbf{K}_L = \mathbf{B}^T \overline{\mathbf{k}} \mathbf{B} + \mathbf{H}_1^T k_\alpha \mathbf{H}_1 + \mathbf{H}_2^T k_\beta \mathbf{H}_2 + \mathbf{H}_3^T k_\gamma \mathbf{H}_3 \tag{17}$$

To complete the derivation, this local stiffness matrix must be transformed to the global coordinate system.

Four-Noded Connector Element

A four-noded interface element suitable for modeling subfloor–joist and ceiling–joist connections is now presented. Consider a typical shell–beam connection, as shown in Fig. 4, which involves two shell elements and a beam element. The beam axis is assumed to be directly beneath the common boundary of the shell elements. The dimensions of this area are equal to the length and width of the beam element. In the following derivations, the shell and beam nodes involved in this connection are denoted by $S1$, $S2$ and $B1$, $B2$, as shown in Fig. 4, whereas the distances from these nodes to the connecting surface at the ith end are denoted by e_{Si} and e_{Bi}. If the shell node is located in the mid-plane and the

beam node is at the center of the cross section, e_{Si} and e_{Bi} are equal to half of the shell thickness and half of the beam depth, respectively.

The local coordinate system is defined as follows: the local x' axis is in the plane of the connecting surface and parallel to the beam axis. The local z' axis is along the normal direction of the shell elements, and the local y' axis is finally computed to complete an orthogonal coordinate system.

After the local coordinate system is established, the relative displacement vector between the bottom surface of the shell and top surface of the beam can be expressed at both ends of the connecting area in terms of the displacements and rotations of the corresponding shell and beam nodes. Assuming that the shell thickness and beam cross-section dimensions do not change during the small elastic deformation, the following displacement relations can be obtained at end 1 for an arbitrary y' coordinate as

$$\begin{Bmatrix} \Delta u_1 \\ \Delta v_1 \\ \Delta w_1 \end{Bmatrix} = \begin{Bmatrix} u_{S1}-u_{B1} \\ v_{S1}-v_{B1} \\ w_{S1}-w_{B1} \end{Bmatrix} + \begin{Bmatrix} -e_{S1}\beta_{S1}-e_{B1}\beta_{B1} \\ e_{S1}\alpha_{S1}+e_{B1}\alpha_{B1} \\ 0 \end{Bmatrix} + y' \begin{Bmatrix} -\gamma_{S1}+\gamma_{B1} \\ 0 \\ \alpha_{S1}-\alpha_{B1} \end{Bmatrix} \tag{18}$$

where (u,v,w) denote displacements along the axes of the local coordinates; and (α,β,γ) indicate rotations about the local axes. Comparing these relations with Eq. (7) in Foschi (1982), it is recognized that the present relations are more general than the one developed by Foschi. In the latter, additional constraints on displacement and rotation variables were assumed as

$$w_{S1}=w_{B1}=w$$

$$\alpha_{S1}=\alpha_{B1}$$

$$\beta_{S1}=\beta_{B1}=\frac{\partial w}{\partial x'}$$

and the normal rotation γ are not considered. The relative displacement vector at end 2 can be obtained using the same method. Assuming a linear variation of relative displacements along the length of the connecting surface, distribution of the relative displacements along the x' coordinate can be expressed as

$$\begin{Bmatrix} \Delta u \\ \Delta v \\ \Delta w \end{Bmatrix} = N_1(x') \begin{Bmatrix} \Delta u_1 \\ \Delta v_1 \\ \Delta w_1 \end{Bmatrix} + N_2(x') \begin{Bmatrix} \Delta u_2 \\ \Delta v_2 \\ \Delta w_2 \end{Bmatrix} \tag{19}$$

where N_i, $(i=1,2)$=linear interpolation functions. Substituting Eqs. (18) into Eq. (19), the relative displacements can be expressed in terms of the nodal displacements and rotations of the shell and beam nodes, $S1$, $S2$ and $B1$, $B2$. The resulting equation can be put into a matrix form as

$$\Delta(x') = \begin{Bmatrix} \Delta u \\ \Delta v \\ \Delta w \end{Bmatrix} = \Delta_1(x') + y'\Delta_2(x') \tag{20}$$

where

$$\Delta_2(x') = \begin{Bmatrix} N_1(x')(-\gamma_{S1}+\gamma_{B1}) + N_2(x')(-\gamma_{S2}+\gamma_{B2}) \\ 0 \\ N_1(x')(\alpha_{S1}-\alpha_{B1}) + N_2(x')(\alpha_{S2}-\alpha_{B2}) \end{Bmatrix} = \begin{Bmatrix} -\Delta\gamma(x') \\ 0 \\ \Delta\alpha(x') \end{Bmatrix} \tag{21}$$

and the expression of $\Delta_1(x')$ can be obtained similarly.

With the expression of the relative displacements and rotations, the strain energy in this shell–beam connection can be obtained. The connectors are assumed to be equally spaced along the length of the contact surface at a distance E_{NL}. Each row may contain multiple fasteners and the ith fastener is located at y_i' in the local y' direction. If the slip moduli of the ith fastener in the local x' and y' directions are $k_{x'i}$ and $k_{y'i}$, and the axial modulus along the local z' direction is $k_{z'i}$, the strain energy can be expressed as

$$U = \frac{1}{2E_{\mathrm{NL}}} \int_L (\boldsymbol{\Delta}_1^T \overline{\mathbf{k}} \boldsymbol{\Delta}_1 + k_\gamma \Delta\gamma^2 + k_\alpha \Delta\alpha^2) dx' \tag{22}$$

where the user-supplied slip and axial moduli have been uniformly smeared over the distance between rows of connectors along the x' direction, and integration in the y' direction has been carried out analytically. The equivalent connector stiffnesses in Eq. (22) are given by

$$\overline{\mathbf{k}} = \sum_i \mathbf{k}_i = \sum_i \begin{bmatrix} k_{x'i} & 0 & 0 \\ 0 & k_{y'i} & 0 \\ 0 & 0 & k_{z'i} \end{bmatrix} = \begin{bmatrix} k_{x'} & 0 & 0 \\ 0 & k_{y'} & 0 \\ 0 & 0 & k_{z'} \end{bmatrix}$$

$$k_\gamma = \sum_i (y_i')^2 k_{x'i} \tag{23}$$

$$k_\alpha = \sum_i (y_i')^2 k_{z'i}$$

When connector stiffnesses are large, the last two terms on the right hand side of Eq. (22) enforce compatibility in normal and axial rotations between the shell and beam elements. This feature is slightly different from Foschi's formulation (1982), where compatibility on axial rotations was explicitly enforced.

Substituting the expressions of $\boldsymbol{\Delta}_1$, $\Delta\alpha$, and $\Delta\gamma$ in terms of the shell and beam nodal displacements and rotations into Eq. (22) and integrating the resulting equation over L along the x' axis, a 24×24 stiffness matrix can be obtained for the four-noded connector element. However, this matrix is defined in the local coordinate system and must be transformed into the global system.

Development of Model

Finite-element formulations for all the elements required in the present model are presented above. These finite elements are used to model the various structural components in a wood-based floor system, including lateral reinforcement, ceiling board, partitions, multilayer floor topping, and beam supports. Because of space limitation, only the modeling of lateral reinforcement is presented here, as this capability is a major improvement over previous floor models.

One of the major advantages of the present finite-element model lies in its ability to model the various types of lateral reinforcements using only the construction parameters such as the mechanical properties of the structural members and the fastener stiffnesses to the joists. All structural members in the lateral reinforcements are idealized by either one or two beam elements. For bridging and bracing, the members are always connected to the joists at the top and bottom of the joist cross sections, as shown in Figs. 2(c and d). For the other three types of lateral reinforcements, the global Z coordinate of the center of the lateral compo-

Table 1. Construction Details of Tested Floor Specimens

Floor No.	Single/double span	Span (m)	Width (m)	Joist type	Joist depth (m)	Joist spacing (m)	Topping and ceiling	Partition wall	Lateral reinforcement type	Boundary condition
1	2	4.88+4.88	4.88	I	0.30	0.610	—	—	—	s-s[a]
2	2	4.88+3.35	4.88	I	0.30	0.610	—	—	—	s-s[a]
3	2	4.88+1.83	4.88	I	0.30	0.610	—	—	—	s-s[a]
4	1	5.90	4.90	Truss	0.24	0.408	—	—	—	s-s[a]
5	1	5.90	4.90	Truss	0.24	0.408	—	—	1 strong back at 1/2 span	s-s[a]
6	1	5.90	4.90	Truss	0.24	0.408	—	—	2 strong back at 1/2 span	s-s[a]
7	1	5.90	4.90	Truss	0.24	0.408	—	—	2 strong back at 1/3 span	s-s[a]
8[c]	1	5.90	4.90	Truss	0.24	0.408	√	—	2 strong back at 1/2 span	s-s[a]
9[e]	1	5.90	4.90	Truss	0.24	0.408	—	√	—	s-s[a]
10[f]	1	5.90	4.90	Truss	0.24	0.408	—	√	—	s-s[a]
11[g]	1	5.90	4.90	Truss	0.24	0.408	—	√	—	s-s[a]
12	1	4.90	4.90	I	0.24	0.488	—	—	—	f-s[b]
13	1	4.90	4.90	I	0.24	0.488	—	—	1 blocking	f-s[b]
14[d]	1	4.90	4.90	I	0.24	0.488	√	—	1 blocking	f-s[b]
15	1	6.25	4.90	I	0.30	0.406	—	—	—	s-s[a]
16	1	6.25	4.90	I	0.30	0.406	—	—	1 brace/strap	s-s[a]
17	1	4.88	3.66	I	0.30	0.610	—	—	—	f-s[b]
18	1	4.88	3.66	I	0.30	0.610	—	—	2 row bridging	f-s[b]
19	1	4.88	3.66	I	0.30	0.610	—	—	1 row bridging	f-s[b]
20	1	4.88	3.66	I	0.30	0.610	—	—	1 bridging/strap	f-s[b]
21	1	7.56	9.35	I	0.41	0.406	—	—	—	s-s[a]
22[d]	1	7.56	9.35	I	0.41	0.406	√	—	—	s-s[a]

[a]s-s=four edges simply supported.

[b]f-s=only two ends of joists simply supported.

[c]Floor No. 8 contains a ceiling of 12.7 mm gypsum board on resilient channel.

[d]Floor Nos. 14 and 22 contain 38 mm concrete floor topping.

[e]Floor No. 9 contains partition wall parallel to joists.

[f]Floor No. 10 contains partition wall perpendicular to joists.

[g]Floor No. 11 contains L-shaped partition wall.

nents must be provided for establishing the geometric relations required by the connector element.

The fastener between each lateral reinforcement member and the joist is represented by the two-noded connector element. The connector stiffnesses required in this element can be specified either by user-defined equivalent stiffnesses or in terms of the locations and stiffnesses of each individual fastener in the connection. In the latter case, equivalent stiffnesses are automatically calculated using Eq. (11). Because the fastener locations and stiffnesses are all defined with respect to the local coordinate system at the connection, the proper definition of these systems becomes very important.

Floor Specimens and Test Procedures

To evaluate the predictive capability of the proposed finite-element model, a series of laboratory tests were conducted on full-size wood-based floors with various structural features, such as gaps in subfloor, topping, partition walls, multispan continuous joists, ceiling, and different types of lateral reinforcements. The measurements included static deflections under a concentrated load, natural frequencies, and mode shapes. Experiments were also carried out to measure mechanical properties of joists and stiffnesses of the fastener–wood connection.

Construction Details of Floor Specimens

A total of 22 full-size floor specimens were constructed and tested. Construction details of the floor specimens are summarized in Table 1. All the floors used composite wood panels as subfloor, i.e., 18.5 mm tongued-and-grooved Canadian softwood plywood (CSP) for floor Nos. 1–3, 12–14, and 21–22; 15.5 mm CSP for floor Nos. 4–11; 18 mm oriented strand board (OSB) for floor Nos. 15–20. Most of the floors used 51 mm screws or nails at an average spacing of 0.3 m along intermediate supports and 0.15 m along edges to attach the subfloor to joists except floor Nos. 12–14 in which glue was used along with nails. For floor specimens with ceiling, gypsum boards were attached to resilient channels on the underside of joists using 30 mm drywall screws and the same nailing schedule as that used for subfloor-to-joist connections. As shown in Table 1, the floor specimens utilized in this paper covered most of the construction details commonly found in current North American construction.

Measurement of Mechanical Properties of Joists and Fastener–Wood Connections

The shear free flexural rigidity (EI) and shear stiffness of the joists were measured before the floor construction using the free–free transverse beam vibration technique developed by Chui

(1991). Equivalent Young's and shear moduli of each joist were then calculated from the measured flexible rigidity and shear stiffness data and utilized in the finite-element analyses.

Both slip and axial moduli of the fasteners are required in the present finite-element model. Experimental data of slip modulus for various types of fastener–wood connections can be found in the literature (Stieda 1990; Mohammad 1996; Ni 1997). For plywood-to-wood, OSB-to-wood, and gypsum board-to-wood, wood-to-wood connections using various types of fastener, the slip modulus reported in these publications varied widely from 3×10^5 to 9×10^6 N/m/fastener, depending on material properties, fastener types, and data analysis techniques.

Because our literature search indicated that there were no published data for nail withdrawal modulus, tests were performed on several types of fastener–wood connections, including the connections between joists and subfloor/ceiling and between joists and the lateral reinforcements. The measured withdrawal modulus varied from 3×10^5 to 1.1×10^6 N/m/fastener. However, these tests were conducted only in withdrawal mode under static loading. With respect to the influence of axial modulus of a fastener on floor response, it is useful to point out that the present model, as in the case of other floor models, assumes that the withdrawal and compression moduli have identical values. For static analysis, there is no difficulty in choosing the proper value of axial modulus because the loading direction is preknown. In the case of frequency analysis, the calculation involves solving for eigenvalues of a system of equations. If different modulus values are to be used, the finite-element equations would be nonlinear and more sophisticated eigensolution techniques must be utilized. This is beyond the scope of the current study. In normal circumstances, the axial modulus is controlled largely by the gripping of the fastener by the wood fiber around the shank of the fastener. As such, the true compression and withdrawal moduli are not expected to differ significantly. If the surfaces of two joining members are in close contact, it may be argued that the apparent compression modulus is higher than the withdrawal modulus due to bearing resistance, and the need to have different modulus values may be justified. However, under serviceability conditions that are of interest here, the load levels experienced by the various floor components are extremely low. Consequently, close tight contact of member surfaces is unlikely to occur, and any axial movement of the fastener in the shank direction is still controlled largely by the gripping force on the fastener and not the bearing stiffness of the wood material. The use of a single modulus value for axial modulus seems reasonable. In addition, as will be shown later, the natural frequency of wood floor systems is generally insensitive to the axial modulus within the practical range.

Measurement of Static Deflections and Natural Frequencies of Test Floors

A number of tests were performed on each floor specimen. Comparison here is limited to static deflection at the floor center under a 1 kN load applied at that location, and the natural frequencies of each floor. In these tests, the static load was applied by a 1 kN dead weight. Natural frequencies were measured using modal analysis technique. Details of the test procedures are available in Hu (1998).

Finite Element Idealization of Test Floors

A sensitivity study was first conducted to determine the adequate finite-element mesh density for accurate prediction of static deflection under a point load and the fundamental natural frequency. This study was based on floor No. 21. The numerical results indicated that the static solution was more sensitive to the mesh density than the natural frequency, but the use of two elements per joist spacing was sufficient for both static and frequency calculations. This meshing rule was then utilized for all test floors considered in the present work. The finite-element mesh, the deformed configuration under the 1 kN point load, and the first free vibration mode shape for floor No. 21 are presented in Fig. 5.

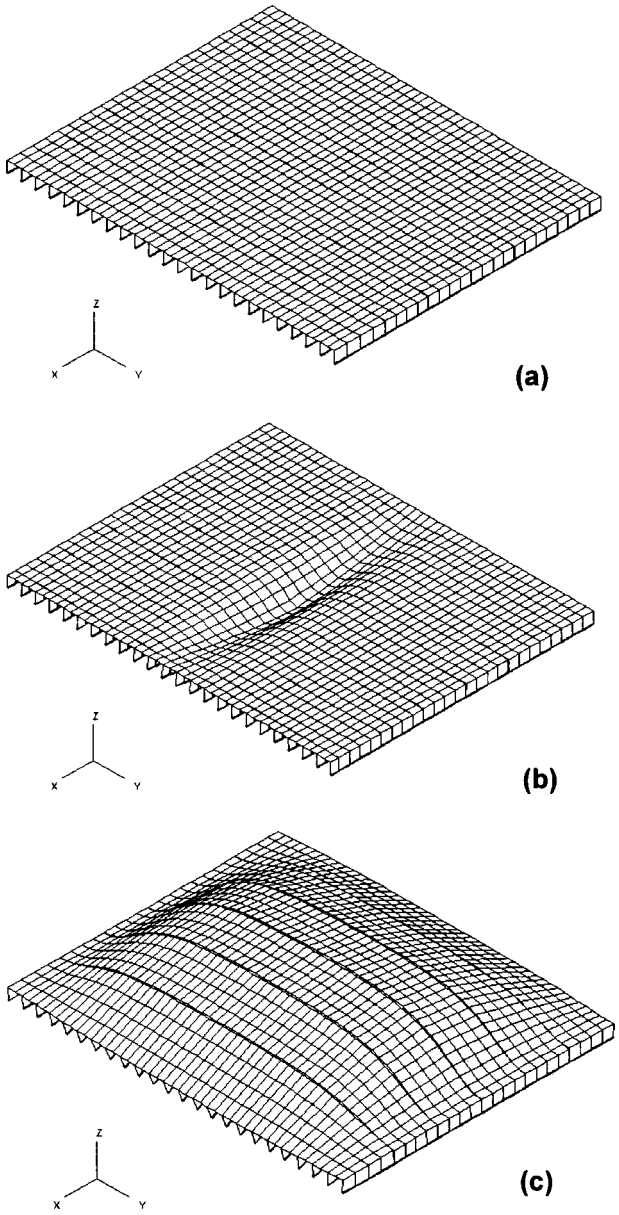

Fig. 5. (a) Finite element mesh; (b) statically deformed configuration; and (c) and first mode shape of test floor No. 21

Sensitivity analyses were then conducted on the slip and axial moduli of the fasteners. Floor No. 21 was still used for these analyses. Fig. 6(a) shows the variation of the predicted static deflection with the slip modulus. In this group of analyses, the axial modulus was fixed at 3×10^8 N/m/fastener. In extreme cases of very small or very large slip modulus, the curve shown in Fig. 6(a) tends to be flat, indicating convergence to the solutions with either zero shear force or zero slip between the joist and subfloor. The range of slip modulus given in the literature is also shown in

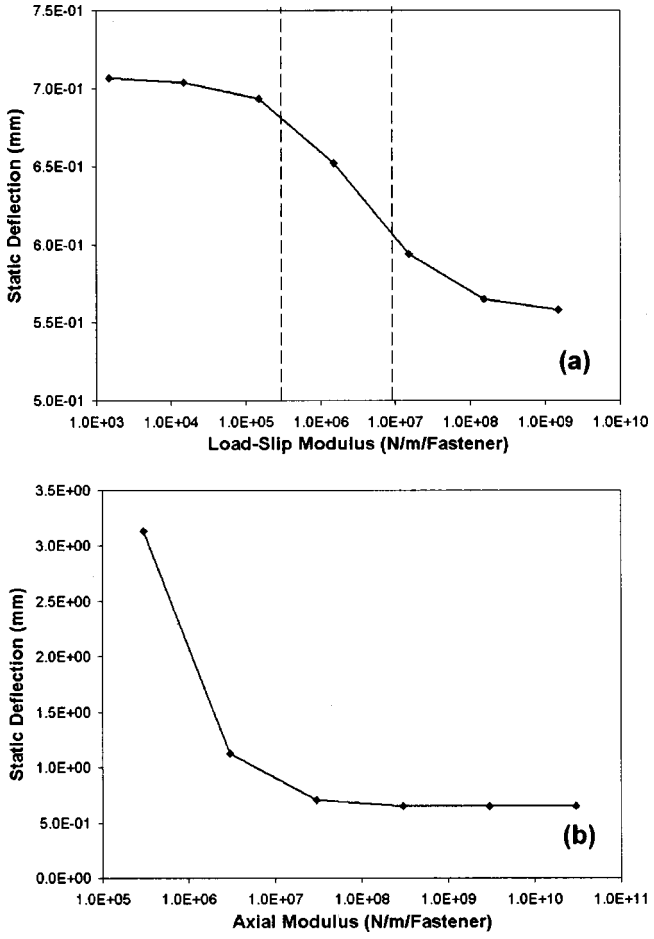

Fig. 6. Results of sensitivity study for static analyses

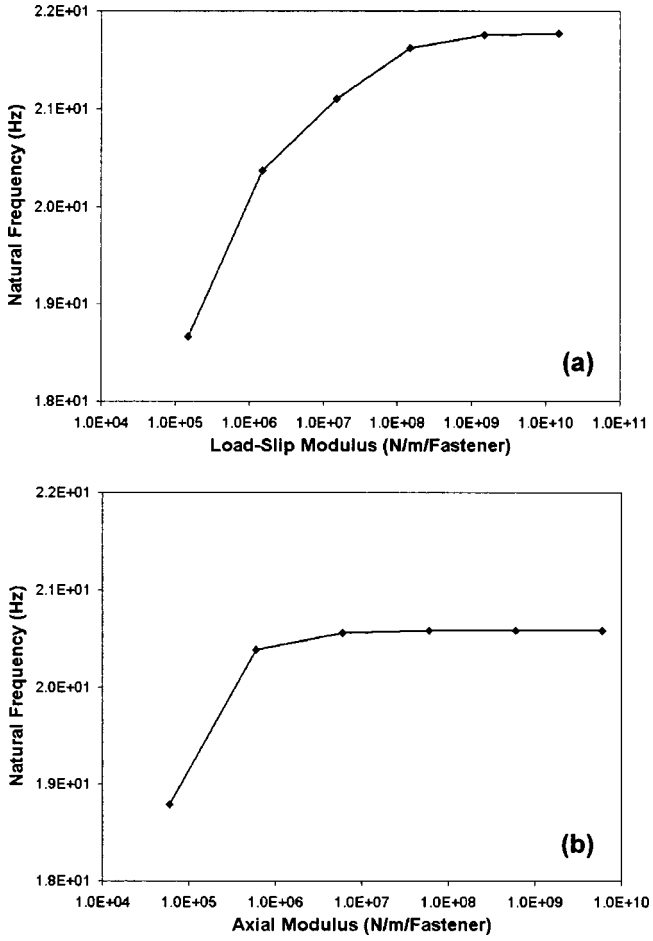

Fig. 7. Results of sensitivity study for natural frequency calculations

this figure, and the present results suggested that the static deflection is sensitive to the value of slip modulus over this range. Based on a comparison of the measured and predicted center deflections, a slip modulus of 1.5×10^6 N/m/fastener was selected and used for all subsequent static solutions in the present paper. The dependence of static deflection of floor No. 21 on the axial modulus is presented in Fig. 6(b), where a constant slip modulus of 1.5×10^6 N/m/fastener has been employed. These results indicated that the static solution is very sensitive to the axial modulus when it is less than 10^7 N/m/fastener. However, with the increase of the axial modulus, the finite-element solution converged to the measured static deflection of 0.68 mm. Based on this observation, an axial modulus of 3×10^8 N/m/fastener was selected for all subsequent static analyses. This axial modulus is several orders of magnitude higher than the withdraw modulus reported earlier in this paper, because in the present analyses, the static load was pointing downward and caused compression instead of withdrawal in the joist–subfloor connection. As a result, a higher axial modulus was expected.

The variations of the predicted natural frequency with the slip and axial moduli were also investigated and the results are presented in Fig. 7. These results indicate that the floor dynamic response is more sensitive to the slip modulus than to the axial modulus within the range of the moduli considered. Through a comparison with the measured fundamental frequency of 21.2 Hz, a slip modulus of 1.5×10^6 N/m/fastener and an axial modulus of 3×10^5 N/m/fastener were selected and used in all natural frequency calculations reported in this paper.

Results and Discussion

The general predictive capability of the present finite-element model was evaluated by comparing the predicted static deflections and fundamental natural frequencies with the measured values for all 22 floor specimens as shown in Figs. 8 and 9. In these figures, the horizontal and vertical axes indicate measured and predicted values, respectively. Each data point represents a test

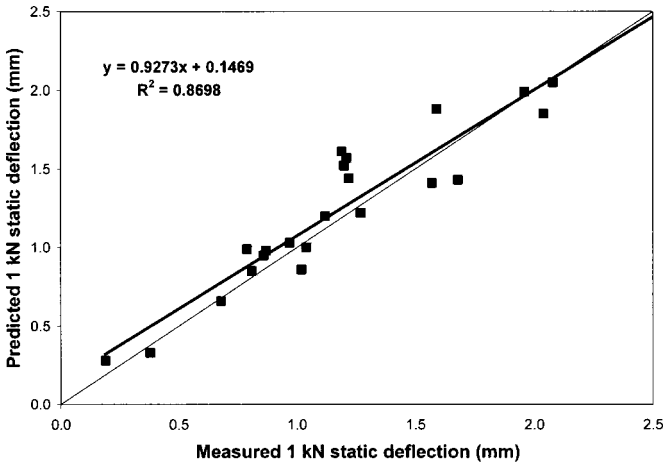

Fig. 8. Comparison of predicted and measured 1 kN static deflections

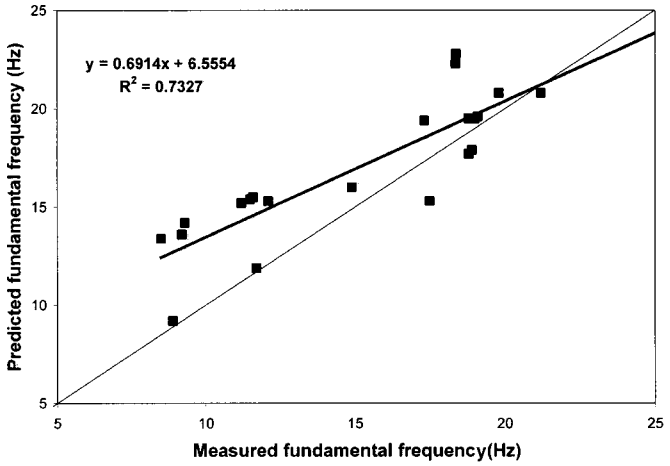

Fig. 9. Comparison of predicted and measured fundamental natural frequencies

floor and the thick solid line is fitted using these points. The thin solid line is a reference corresponding to the ideal situation, in which the measured and predicted results are identical. As can be observed, the predicted static deflections matched the measured values well. However, the predicted fundamental natural frequencies were generally higher than the measurements. This might be caused by the fact that the support conditions of the laboratory-built floor specimens were not rigid simple supports, as assumed in the finite-element calculations. The flexibility in supports affects fundamental natural frequencies significantly, especially for floors with short spans.

To verify this hypothesis, additional finite-element analyses were performed on floor No. 4 using flexible boundary conditions. In the actual experiment, the ends of the joists were nailed to wood-supporting walls. Such support conditions prevented downward displacements of the joist ends. However, uplift could occur due to nail withdrawal in the frequency tests. To simulate the potential uplift of the joist ends, boundary springs with a finite stiffness of 2×10^5 N/m were employed for the support restraints in the finite-element model to predict the fundamental natural frequency. This value was based on nail withdrawal tests described above. After using the more realistic boundary conditions, the predicted fundamental natural frequency was reduced to 11.5 from 15.2 Hz. The new result is in a much closer agreement with the measured value of 11.2 Hz.

It should be noted that the 22 floors covered a broad range of construction details that have provided an evaluation of the general predictive capability of the proposed floor model. To closely examine the ability of the proposed finite-element model in accounting for the contribution of lateral reinforcements to floor performance, the measured and predicted changes in static deflections and fundamental frequencies of eight floor specimens due to installation of lateral reinforcements are compared in Table 2. The percentage changes are presented instead of the actual values to provide a meaningful evaluation of the proposed modeling approach by eliminating the influence of other factors that may cloud the evaluation. As can be observed, the predicted changes in static deflections and fundamental natural frequencies due to the installation of the lateral reinforcements matched the measured changes quite well. A review of these results shows that the addition of a lateral reinforcement generally leads to a small increase in the first natural frequency, but a large reduction in static deflection. In general, using the assumed slip and axial moduli presented in the preceding section, the proposed finite-element model slightly underestimates the contributions from these lateral reinforcements, which makes the predicted results conservative. Considering the uncontrollable workmanship in the installation of the lateral reinforcements on site, a conservative approach would be preferable for accounting for the contributions of these structural components. Such a conservative approach can prevent excessive vibrations in floors caused by an overestimation of the contributions from lateral reinforcements.

Conclusions

In this paper, a finite element procedure for linear static and natural frequency analysis of wood-based floor structures is presented. The implementation of the present model has been based on an existing finite element program *VAST*. A numerical verification of the developed finite-element capability was carried out using a number of wood-based floors. The predicted static deflections and fundamental natural frequencies were compared with the measured data and they were found to be in good agreement.

Based on the verification results, the finite-element model presented in this paper is reliable and unique, particularly in modeling wood-based floor structures with various types of lateral reinforcements. The main benefit of the present model comes from its use of only the stiffness of the structural members and the mechanical properties of the connections to achieve good predictions for static and dynamic behavior of wood-based floors. The stiffness of structural components in the lateral reinforcements and the mechanical properties of the connections all can be determined experimentally. This special feature makes the present model a useful tool not only for wood-based floor performance research and design, but also for developing new wood-based floor construction products and systems.

Table 2. Comparison of Measured and Predicted Contributions of Various Lateral Reinforcements to Floor Performance

Floor No.	Measured change in frequency (%)	Predicted change in frequency (%)	Measured change in deflection (%)	Predicted change in deflection (%)	Lateral reinforcement type
5	2.7	1.3	−46.2	−41.5	1 strong back at 1/2 span
6	2.7	1.3	−53.4	−49.8	2 strong backs at 1/2 span
7	3.6	2.0	−38.9	−40.5	2 strong backs at 1/3 span
13	0.5	1.1	−45.3	−47.9	1 row of blocking at 1/2 span
16	9.4	6.0	−19.9	−29.1	1 row of bracing/strapping at 1/2 span
18	0.5	0.5	−35.2	−31.3	2 rows of bridging at 1/3 span
19	−1.1	0.0	−14.8	−30.6	1 row of bridging at 1/2 span
20	4.2	6.7	−33.6	−41.0	1 row of bridging/strapping at 1/2 span

Acknowledgments

The writers would like to thank the Canadian Forest Service (Natural Resources Canada) and the Natural Sciences and Engineering Research Council of Canada for their financial support of the research projects from which information presented in this paper was extracted.

References

Ahmad, S., Irons, B. M., and Zienkiewicz, O. C. (1970). ''Analysis of thick and thin shell structures by curved finite elements.'' *Int. J. Numer. Methods Eng.*, 2, 419–451.

Beattie, G. J. (1998). ''The vibration performance of timber floors.'' *Study Rep. No. 79*, Branz–the Resource Center for Building Excellence, Auckland, New Zealand.

Berkoh, F. O. (1997). ''Occupant-induced vibration in wood floors: A serviceability approach.'' PhD thesis, Carleton Univ., Ottawa.

Chui, Y. H. (1987). ''Vibration performance of wooden floors in domestic dwellings.'' PhD thesis, Brighton Polytechnic, Brighton, U.K.

Chui, Y. H. (1991). ''Simultaneous evaluation of bending and shear moduli of wood and the influence of knots on these parameters.'' *Wood Sci. Technol.*, 25(2), 125–134.

Dvorkin, E. N., and Bathe, K. J. (1984). ''A continuum mechanics based four-node shell element for general nonlinear analysis.'' *Eng. Comput.*, 1, 77–88.

Filiatrault, A., Folz, B., and Foschi, R. O. (1990). ''Finite-strip free-vibration analysis of wood floors.'' *J. Struct. Eng.*, 116(8), 2127–2142.

Folz, B., and Foschi, R. O. (1991). ''Coupled vibrational response of floor system with occupants.'' *J. Eng. Mech.*, 117(4), 872–892.

Foschi, R. O. (1982). ''Structural analysis of wood floor systems.'' *J. Struct. Div. ASCE*, 108(7), 1557–1574.

Foschi, R. O., and Gupta, A. (1987). ''Reliability of floors under impact vibration.'' *Can. J. Civ. Eng.*, 14(5), 683–689.

Gupta, A. (1985). ''Reliability of floors under impact vibration.'' MSc thesis, Univ. of British Colombia, Vancouver, B.C., Canada.

Hu, L. J. (1992). ''Prediction of vibration responses of ribbed plates by modal synthesis.'' PhD thesis, Univ. of New Brunswick, Fredericton, N.B., Canada.

Hu, L. J. (1998). ''Appendix: Protocols for field testing of wood-based floor systems.'' *Rep. No. 3 on Serviceability Design Criteria for Commercial and Multi-family Floors*, Forintek Canada Corp., Sainte-Foy, Que., Canada.

Martec Limited. (2000). *Vibration and strength analysis program (VAST) user's manual*, Halifax, Nova Scotia, Canada.

McCutcheon, W. J. (1977). ''Method for predicting the stiffness of wood-joist floor systems with partial composite action.'' *Research Paper No. 289*, Forest Products Laboratory, USDA Forest Service, Madison, Wis.

Mohammad, M. (1996). ''Stiffness responses of nailed OSB-to-lumber connections: Influence of moisture conditioning and load cycling.'' PhD thesis, Univ. of New Brunswick, Fredericton, N.B., Canada.

National Research Council (NRC). (1995). ''National Building Code of Canada.'' Ottawa.

Ni, C. (1997). ''Behavior of nailed timer joints under reversed cyclic load.'' PhD thesis, Univ. of New Brunswick, Fredericton, N.B., Canada.

Onysko, D. M. (1981). ''Deflection of floors under concentrated loadings.'' *Rep. of Project No. 12*, Canadian Forest Service, Forintek Canada Corp., Ottawa.

Przemieniecki, J. S. (1968). *Theory of matrix structural analysis*, McGraw-Hill, New York, 74–74.

Smith, I. (1980). ''Series type solutions for built-up timber beams with semi-rigid connections.'' *Proc. Inst. Civ. Eng., Struct. Build.*, 2(69), 707–719.

Stieda, C. K. A. (1990). ''The lateral resistance of nailed plywood-to-wood connections.'' *Rep. Prepared for Project VP-X-177*, Forintek Canada Corp., Vancouver, B.C., Canada.

Thompson, E. G., Goodman, J. R., and Vanderbilt, M. D. (1975). ''Finite element analysis of layered wood systems.'' *J. Struct. Div., ASCE*, 101(12), 2659–2672.

Vermeyden, P. (1968). ''Research into the load sharing action of the decking of a wooden floor in concentrated load.'' *Rep. of Translation No. 41*, Dept. of Fisheries and Forestry, Eastern Forest Products Laboratory, Ottawa (in Dutch).

Young, W. C., and Budynas, R. G. (2002). *Roark's formulas for stress and strain*, McGraw-Hill, New York, 166–167.